Principles and prospects of direct high resolution electron image acquisition with CMOS detectors at low energies

2009 J. Phys.: Condens. Matter 21 314004

(http://iopscience.iop.org/0953-8984/21/31/314004)

J. Phys.: Condens. Matter **21** (2009) 314004 (9pp) doi:10.1088/0953-8984/21/31/314004

Principles and prospects of direct high resolution electron image acquisition with CMOS detectors at low energies

A R Faruqi

MRC Laboratory of Molecular Biology, Hills Road, Cambridge CB2 0QH, UK

E-mail: arf@mrc-lmb.cam.ac.uk

Received 9 December 2008
Published 7 July 2009
Online at stacks.iop.org/JPhysCM/21/314004

Abstract
Two types of direct electron detectors, potentially useful in low energy electron microscopy and photoemission electron microscopy (LEEM/PEEM) experiments, are reviewed in this paper. Hybrid pixel detectors, using a silicon sensor and based on Medipix2 offer a high detective quantum efficiency, due to an essentially noiseless readout, but are technically challenging. Backthinned monolithic active pixel sensors (MAPS) are not noise-free but have other advantages as discussed in this review.

1. Introduction

During the past decade microelectronics technology has advanced to such an extent that it has become feasible to design CMOS detectors with high efficiency for recording electrons with energies suitable for electron microscopy (Faruqi and Henderson 2007). Electronic detectors for electron microscopy have previously been based on phosphor coupled fibre optics CCD technology. Due to shortcomings in the performance of CCD detectors, however, we have investigated two new types of direct detectors, which use direct detection in silicon rather than converting the electron energy into light imaged by the CCD. The two direct detectors, described more fully below, are hybrid pixel detectors (HPDs) and monolithic active pixel sensors (MAPS). Although detectors for our work in electron cyo-microscopy requires energies of 100–300 keV, similar detectors, with certain provisos can be used effectively for recording electrons with lower energies in the range 6–35 keV, which are of interest to the LEEM/PEEM community. Since we deal exclusively with direct electron detection, previous methods for low energy electron detection using indirect methods such as those based on microchannel plates are not covered by this review.

2. Electron detection in silicon: special problems at low and high energies

The detection of electrons, or indeed of any ionizing radiation in a semiconductor material such as silicon, relies on the generation of electron–hole pairs, either of which could be collected and used as the signal. Electrons move freely in the conduction band under the influence of an applied external electric field to the electrodes where the charge can be amplified and detected. The signal generated depends on the semiconductor properties of silicon: the energy of the band gap for silicon is 1.12 eV, and the energy required to produce an electron–hole pair is ∼3.55 eV. The key feature, which allows silicon to be converted into a position sensitive detector or an imaging device, is that it can be divided into a large number of independent picture elements or pixels (Faruqi and Subramaniam 2000).

As the incident electron traverses in silicon it undergoes both elastic and inelastic scattering. The former results in a change in direction with no energy loss but the latter leads to both a smaller change in direction and energy loss. The trajectory of electrons in silicon can be simulated by employing a Monte Carlo program of which an example is given in Joy (1995). McMullan *et al* have published simulations based on Monte Carlo simulations which, in addition to predicting the trajectory, also estimate the amount of energy deposited along the electron track for incident energies between 100 and 300 keV (McMullan *et al* 2007, 2008). The simulated trajectory of electrons at 120, 200, and 300 keV in silicon and 300 keV in a more dense sensor material, CdTe, is given in figure 1. The faint vertical stripes are drawn at a spacing of 55 μm and are equal to the pixel size in the Medipix2 detector (Llopart *et al* 2002). An important point to note from these simulations is that, at 120 keV, the lateral extent of the

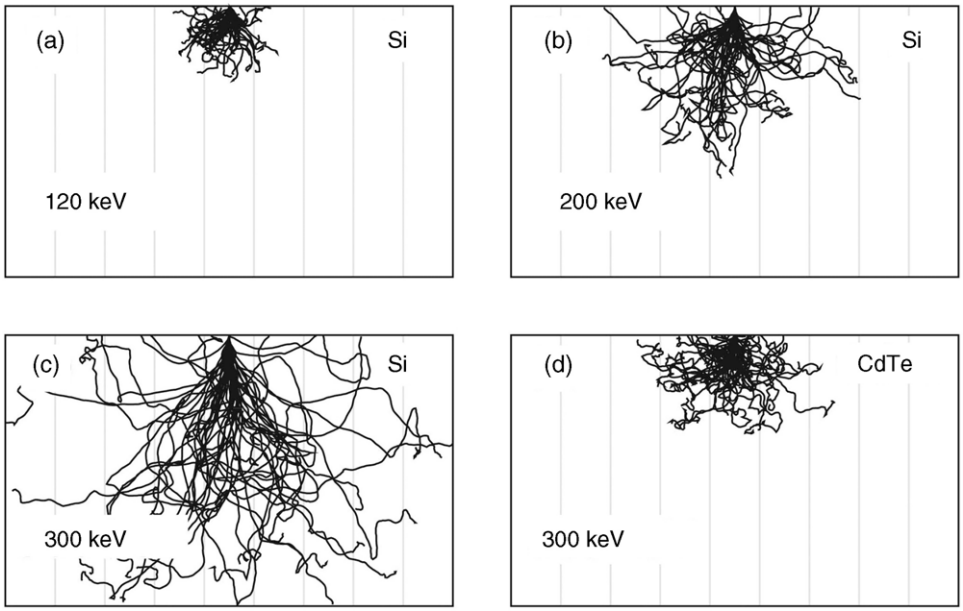

Figure 1. (a)–(d) Monte Carlo simulations showing electron trajectories in silicon with the energies of the incident electron set at 120, 200, and 300 keV. For comparison, electron trajectories in CdTe are shown at 300 keV; note the much smaller lateral spread in charge for the same energy compared to silicon. Reproduced with permission from McMullan *et al*. Copyright 2007 by Elsevier.

electron trajectory is approximately contained within one pixel. At higher energies the electron trajectory crosses over into a number of pixels, thus reducing the spatial resolution of the detector. It can also be seen that higher energies could be detected with good resolution if a more dense material, such as cadmium telluride (CdTe) or gallium arsenide (GaAs) were used instead of silicon for the sensor. The lateral spread of the charge in CdTe at 300 keV is less than the lateral spread at 200 keV in silicon. It follows that at lower energies (5–35 keV), the incident electron has a far smaller range in silicon and is likely to be contained in one pixel unless, as a special case, it lands on an inter-pixel boundary.

Cabello and Wells (2007) have published simulations for the range of lower energy electrons (<80 keV) in silicon which were performed for modelling the MAPS sensor behaviour for tritium auto-radiography. The mean energy of electrons is 5.7 keV with the end-point at 18.6 keV (Deptuch 2005). However, the simulations on low energy electrons are just as relevant for LEEM/PEEM applications, which deal with electrons in a similar energy range. As can be seen from the electron range curves as a function of energy in figure 2, it is difficult for electrons with the lowest energy (5 keV), to penetrate into the sensitive volume as the range is only 0.2 μm. Even at 10 keV the range is less than 1 μm, much less than the typical passivation layer thickness for MAPS sensors. The Al metal coating on the Medipix2 sensor however, is less than 1 μm in thickness and it should be able to detect electrons with energies of less than 10 keV and indeed this is the case (Mettivier *et al* 2004). Given a passivation layer thickness of $\sim$5 μm, the minimum energy electrons which could be detected in a normal MAPS sensor is about 30 keV. As discussed in more detail below, this involves backthinning MAPS sensors and back-illuminating them to circumvent this problem.

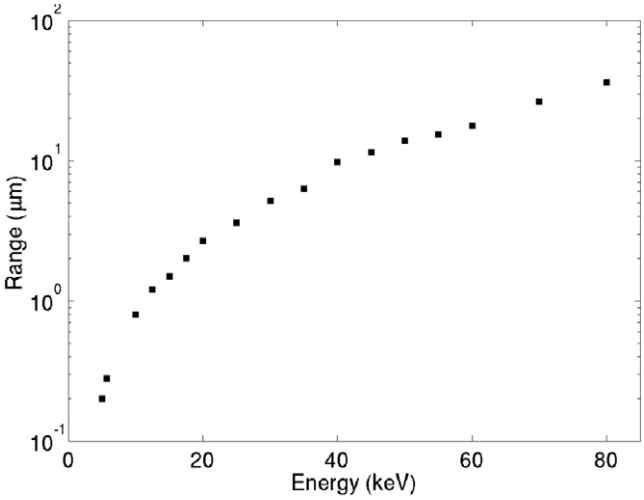

Figure 2. Range of low energy electrons in silicon calculated from Monte Carlo simulations. Reproduced with permission from Cabello and Wells. Copyright 2007 IEEE. It can be seen that even at the higher end of the energy of interest, namely 35 keV, the range is $\sim$5 μm, which is about the passivation layer thickness in a MAPS detector—hence the need for backthinning and back-illumination.

We describe hybrid and MAPS based detectors followed by some general conclusions.

3. Hybrid pixel detectors

Hybrid pixel detectors (HPDs) contain a pixellated sensor layer made of high resistivity p–i–n silicon, in which pixels are individually bump bonded to a readout electronics chip, with the same pixellation; the pixels are patterned on the p side of the sensor. The results on hybrid detectors discussed here

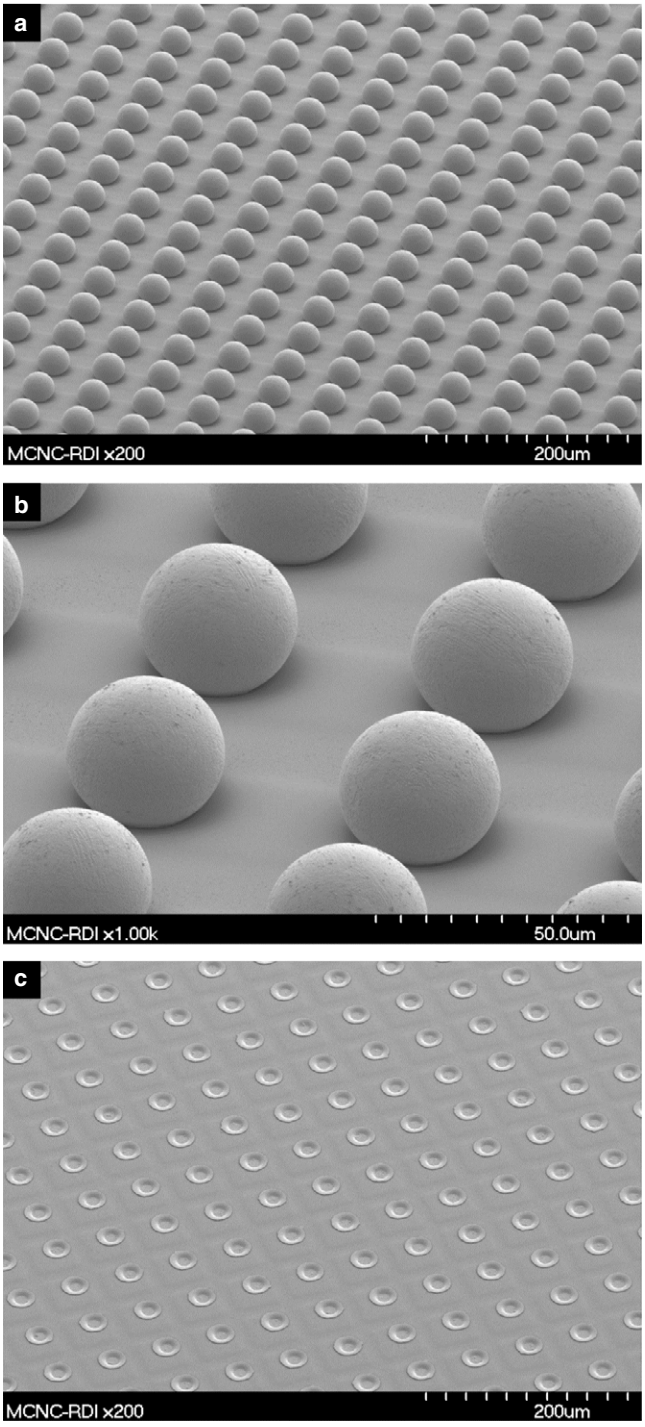

Figure 3. (a)–(c) Images of solder bumps placed on the readout chip (a) at intervals of 55 μm and at higher magnification in (b). Metallization of the sensor layer is shown in (c).

were all obtained using the Medipix2 chip, developed within the Medipix collaboration based at CERN (http://medipix.web.cern.ch/MEDIPIX, Llopart and Campbell 2003). The basic Medipix2 chip contains 256×256 55 μm pixels and a 2×2 tiled array (Quad) contains 516 pixels × 516 pixels. The detectors described in these tests had a 300 μm thick silicon sensor.

Prior to bump bonding solder bumps are deposited on the electronics chip surface and the sensor chip is metallized.

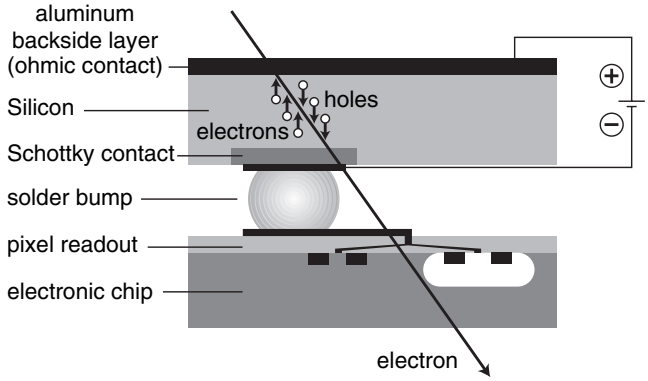

Figure 4. Schematic diagram of a single Medipix2 pixel with the sensor and readout separated by a bump bond. The aluminium layer forming the ohmic contact is only a fraction of 1 μm, making it more convenient for the detection of low energy electrons.

Bonding between the two chips takes place subsequently when the two surfaces are pushed together at a temperature high enough to melt the solder. The process of bumpbonding requires special tools and skills and, due to these technical difficulties can, in some instances, lead to a higher than acceptable failure rate. Images of the solder drops deposited on the readout chip (courtesy of R LaBennett, RTI International, NC, USA) at intervals of 55 μm, the pixel pitch, are shown in figure 3(a) and at a higher magnification in figure 3(b). The solder diameter is approximately 20 μm, occupying a significant fraction of the available area in a pixel. The sensor layer, shown in figure 3(c), needs metallization prior to the bonding process, completing the electrical connection between the sensor and the readout electronics.

When a suitable (∼100 V) voltage field is applied across the sensor there is complete depletion in the sensor volume. An electron incident on the sensor loses energy, resulting in the production of electron–hole pairs; they are free to drift in the potential created by the applied voltage—for silicon, holes are often used for the signal. An electron with 120 keV energy creates ∼33 000 electron–hole pairs in the detector layer and, due to the long lifetime of holes in silicon, a large fraction are collected at the detector node. As we will see later, the pixel amplifier readout noise is typically 100e^- rms (Tlustos *et al* 2006), leading to an excellent signal-to-noise (SNR) of >300, which can be utilized in noise-free acquisition of images (Faruqi *et al* 2003, 2005b, McMullan *et al* 2007, Faruqi and Henderson 2007, Faruqi 2007, McMullan and Faruqi 2008). This should also be true at much lower incident electron energies, of interest to LEEM (30 keV), and a high SNR should be achievable to permit noise-free imaging (Faruqi *et al* 2005b).

The schematic diagram of a single Medipix2 pixel is shown schematically in figure 4. A thin aluminium layer is coated on the top side and a Schottky contact on the readout side to be able to apply a potential across the sensor; with a potential of 50–100 V the sensor is fully depleted. Pixel level electronics is used to shape and amplify the signal before discriminating against noise pulses as shown in figure 5. The electronics can be broadly divided into a front-end analogue

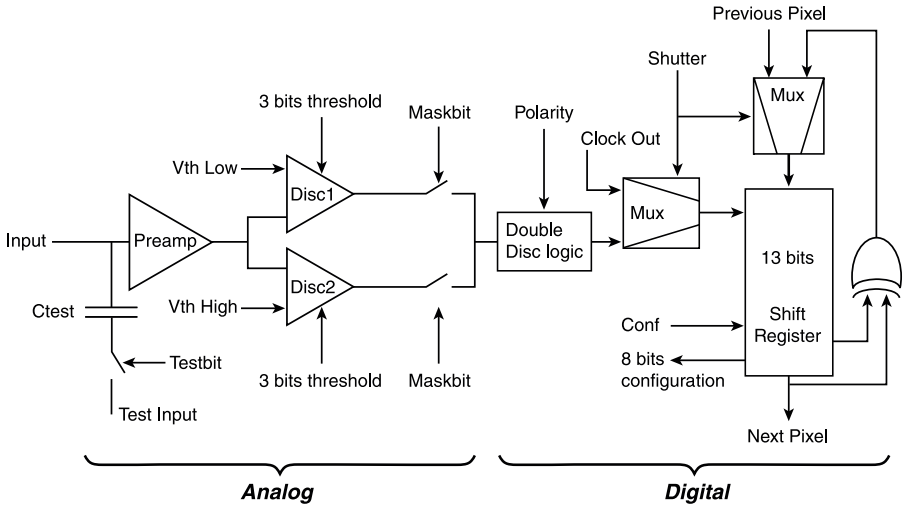

Figure 5. Single pixel electronics for the readout in Medipix2. Reproduced with permission from Llopart and Campbell. Copyright 2003 Elsevier.

part and a rear-end digital part. The signal from the incident electron is amplified and compared against two preset voltage levels: a lower level threshold which is used to eliminate noise (also used to optimize the detector performance at different energies) and an upper level threshold, which is not needed for monochromatic electrons. Accepted signal pulses are counted in a 13-bit shift register, which is read out sequentially with other pixels at the conclusion of the image acquisition.

A special feature of Medipix2, which helps in improving the uniformity of response over the whole sensitive area, is the ability to set two different types of thresholds: a global threshold covering all pixels and a local threshold specific to individual pixels. The latter threshold setting relies on a three-bit digital to analogue converter (DAC) used to fine-tune the threshold value for optimum uniformity, which minimizes the small pixel-to-pixel non-uniformities (Tlustos *et al* 2006). This procedure is particularly important for low energy electron detection as it allows the global threshold to be set at the lowest possible value without compromising SNR. According to Mettivier *et al* 2004, who used Medipix2 for tritium-based auto-radiography, when special care is taken with equalizing thresholds, it is possible to set the lower threshold to 6–7 keV. Since the background noise counts at these settings were comparable to the cosmic ray background, the detector could be used as a very efficient electron detector for fairly low energy electrons.

Due to the high scattering power of any potential window material, any detector used for electron microscopy needs to operate in the high vacuum environment of the camera chamber. Since the bulk of the readout system for electronic detectors is located externally to the camera chamber it is necessary to use high vacuum compatible feed-throughs to control the operations of the detector (Faruqi and Subramaniam 2000).

Another important issue related to the practical use of the detector is the problem of radiation damage. Radiation damage due to electron irradiation in Medipix2 can be divided into two distinct parts: below about 250 keV damage appears minimal but at 300 keV, and presumably above, the readout chip is affected. The sensor part of the detector should not suffer radiation damage at the energies we are working at and this is born out by experiments (Faruqi *et al* 2005b, McMullan *et al* 2007). However, the readout chip can be damaged by radiation, probably due to the increased leakage currents in diodes as has been discussed previously in the context of CMOS detectors (Faruqi *et al* 2006). The sensor acts as an effective shield by stopping electrons with an energy of up to about 250 keV but damage is evident at 300 keV (McMullan *et al* 2007). This is confirmed by simulations shown in figure 1, which predict that a small fraction of the incident electrons would be able to penetrate through the 300 μm sensor layer and impinge on the readout chip causing damage. Some of the electronics on the readout board also need to be shielded from the incident radiation and a metal shield with a rectangular aperture was used for the shielding. Two examples of the Medipix2 mounting in two different microscopes are shown in figures 6(a) and (b); (a) shows the mounting of a single chip in a 120 keV CM12 electron microscope and (b) shows a quad mounting setup in a 300 keV FEI Tecnai microscope.

3.1. Modulation transfer function (MTF) and detective quantum efficiency (DQE)

Using the knife-edge method, the MTF of Medipix2 was measured as a function of global threshold at 40, 80 and 120 keV (McMullan *et al* 2007). The MTF curves shown in figure 7(a) are a summary of the MTF at Nyquist frequency at the three electron energies and a more conventional curve showing MTF as a function of spatial frequency at 120 keV with a 60 keV threshold is shown in the inset.

As mentioned earlier, the range of electrons is about equal to the pixel size, roughly 55 μm, at 120 keV and is correspondingly smaller at lower energies. By setting an appropriate threshold it is possible to reduce noise and events which deposit a small amount of energy in a given pixel, without sacrificing efficiency. As shown in the Monte Carlo simulations for the range of electrons in silicon, at 30 keV the

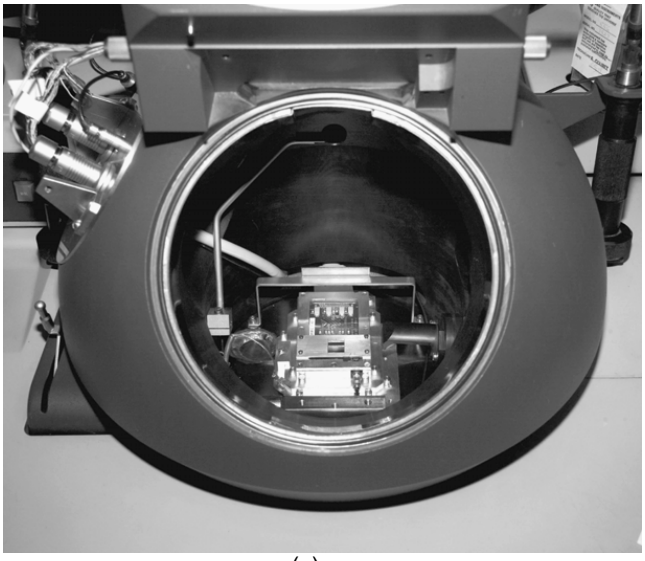

(a)

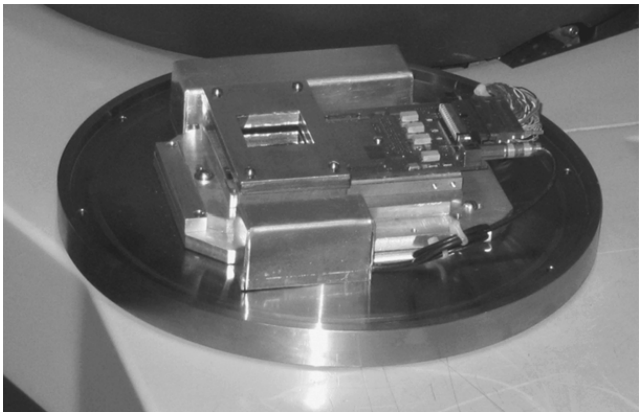

(b)

Figure 6. (a) Photograph of the single-chip Medipix2 mounting in the CM12 120 kV electronmicroscope. Reproduced with permission from Faruqi *et al* (2005b). Copyright 2005 Elsevier. (b) Photograph of the quad detector in a specially constructed mounting prior to installation in the Tecnai F30 300 kV electron microscope. Reproduced with permission from McMullan *et al*. Copyright 2007 Elsevier. In both cases a metal shield with a square hole is used to protect auxiliary electronics from radiation.

range is only ∼5 μm. Very good agreement has been obtained between the experimental values of MTF, drawn as symbols, and the results of Monte Carlo simulations, which are drawn as continuous lines.

The DQE of a detector is defined as:

$$\mathrm{DQE} = (\mathrm{S/N})^2_{\mathrm{output}}/(\mathrm{S/N})^2_{\mathrm{input}}$$

where S and N refer to the signal and noise respectively. Since the value of S/N at the output is always smaller than S/N at the input, DQE is always less than 1. The DQE at different spatial frequencies is given by the following equation (McMullan *et al* 2007):

$$\mathrm{DQE}(\omega) = \mathrm{DQE}(0) \times \mathrm{MTF}(\omega)^2/\mathrm{NTF}(\omega)^2$$

where NTF is the noise transfer function. Figure 7(b) shows the experimentally observed DQE(ω) as a fraction of the maximum possible value as triangles along with the theoretically predicted values drawn as a continuous line. The dotted line gives the actual experimental values for DQE(ω). An outstanding feature of Medipix2 is the high value of DQE obtained even with very low dose images—which is not possible with detectors that do not rely on counting.

3.2. Application of Medipix2 in noiseless imaging

An example of the noiseless readout of Medipix2 is illustrated in the following example. Images of negatively stained rotavirus were obtained at extremely low doses at a magnification of 66 000 as shown in figure 8(a). The dose was 1.6 electrons/pixel which corresponds to 0.04 electron Å^{-2} at the sample. The sum of a series of 100 images, with 1 s exposure for each image, is shown in figure 8(b). Due to the drift in the specimen stage, the individual images were aligned according to the procedure described in the reference (McMullan and Faruqi 2008). The total electron dose on the specimen was 4 electrons Å^{-2}, equivalent to the dose typically used for electron cyo-microscopy.

4. CMOS detectors

As mentioned earlier the sensor and readout parts for monolithic active pixel sensors (MAPS) are located in the same layer as shown for a pixel in figure 9. This makes the design somewhat simpler as it eliminates the need for bump bonding between the sensor and readout chips. Since the design is based on commonly used CMOS technology, several attractive features can be incorporated in the detector, such as diodes, transistors, ADCs etc and CMOS technology used over the past decade or so originally for use as the sensor in digital cameras and other consumer products (Prydderch *et al* 2003). A number of enhancements, listed below, to the 'consumer' CMOS devices is needed to convert them into efficient electron detectors.

First, to increase the signal from the incident electrons an additional epitaxial layer (epilayer) is added to the sensor. Second, the electronics components in the readout, such as diodes and transistors need to be radiation hardened to operate over a reasonable timescale. Third, the detector can only be used for low energy electrons by backthinning the sensor and using back-illumination, as discussed in recent publications (Cabello *et al* 2007, Deptuch 2005). Four, the original sensors for light had different requirements in terms of pixel size—electron detection requires larger pixels. Five, due to the larger pixel size and the requirement for a large number of pixels in the detector, it is necessary to employ stitching of several sensors to achieve a sufficiently large area.

The operation of a MAPS detector can be understood more clearly from the layout of a single MAPS pixel, shown schematically in figure 9. The sensor consists of a thin sensitive (4–20 μm) lightly doped layer of silicon, the epilayer, above a thick, heavily p-doped (inert) layer of silicon. The latter does not play any part in the detection or readout but provides mechanical rigidity and support for the detector. Above the epilayer is a passivation layer, which together with the

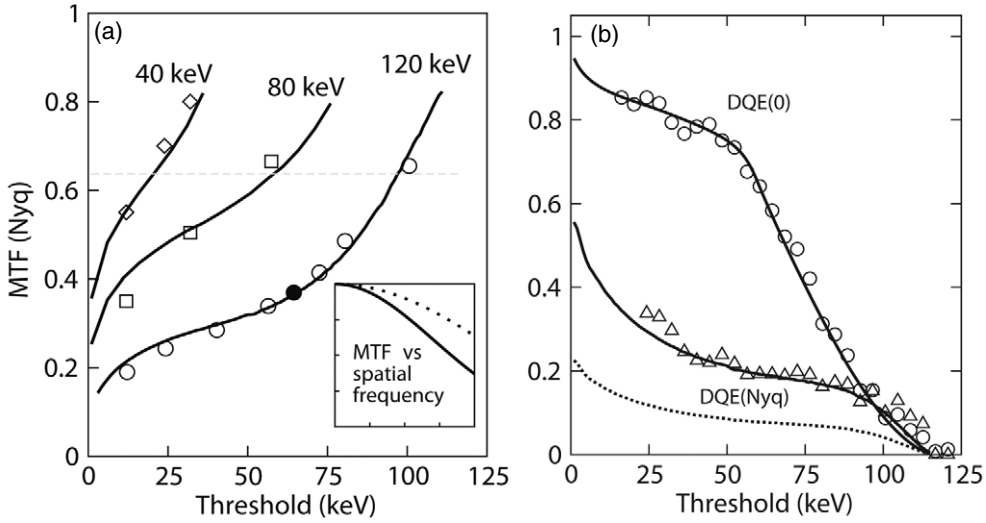

Figure 7. (a) Experimental and theoretical values of MTF as a function of global threshold for Medipix2 at 40, 80 and 120 keV. (b) Experimental and theoretically calculated values of DQE(0) and DQE(ω) as a function of global threshold. Reproduced with permission from McMullan *et al*. Copyright 2007 by Elsevier.

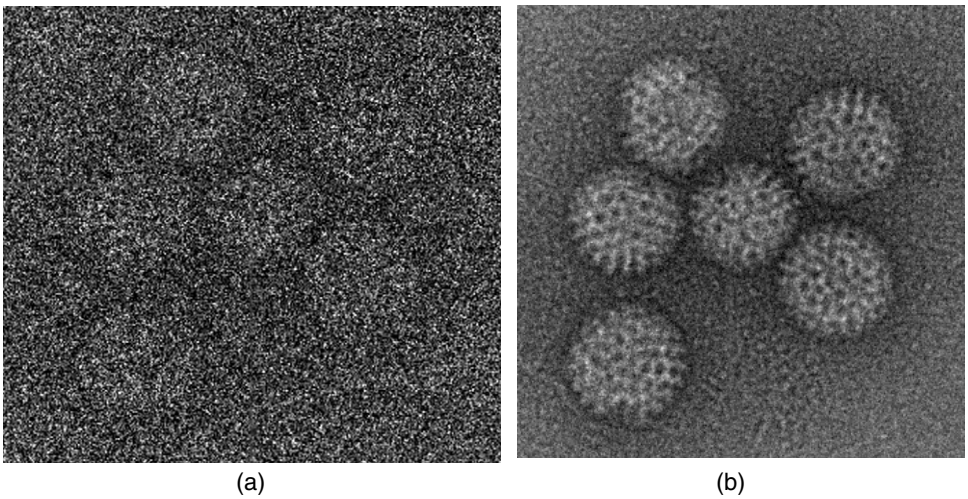

Figure 8. Rotavirus images recorded at different electron dose levels. (a) Top left. Rotavirus image with only ∼1.5 electron/pixel. (b) Top right. Sum of 100 images shown in (a) after alignment, which is essential as there is considerable drift in the image over the 100 exposures. Reproduced with permission from McMullan *et al*. Copyright 2008 Elsevier.

electronics is about 5 μm in total thickness—this needs to be traversed by an incident electron prior to entering the epilayer. Backthinning to the epilayer and then illuminating from the reverse side ensures that even electrons with energy as low as 5 keV are detected in the epilayer (Deptuch *et al* 2007, Faruqi 2007, http://mi3.shef.ac.uk/).

The readout electronics, consisting of one or more collection diodes and several transistors are implanted above the epilayer. The different doping levels in the diode, epilayer and substrate generate an inherent potential which leads to charge (electrons) diffusing to the diode. The electrons are generated by, and constitute the signal due to, the incident electron. As there is no potential applied externally, electrons are collected on the diode purely by diffusion in the epilayer. Electrons diffusing toward the p^{++} bulk layer are reflected back into the epilayer due to the potential difference at the boundary; electrons diffusing toward the n^+ region are trapped in a potential well and unable to escape. The sequence of events is as follows: the diode capacitance gets charged up at the beginning of the exposure and discharged by the signal electrons during the exposure. One of the pixel transistors controls the readout, which is digitized externally in an analogue-to-digital converter (Prydderch *et al* 2003). The readout from a pixel can be explained with reference to figure 1 (Faruqi 2007, Faruqi and Henderson 2007). Prior to exposure the node A, at the output of the n^+ diode, is reset to a fixed positive voltage by the transistor T1. During exposure, electrons collected through the n^+ diode discharge the stored value by a small amount, which represents the signal to be recorded. During readout, columns are selected sequentially and all pixels in a given row are read out (the row is selected by the transistor T3) through transistor T2. The small signal from the pixel is amplified and then digitized in an ADC in circuits usually separate from the detector chip.

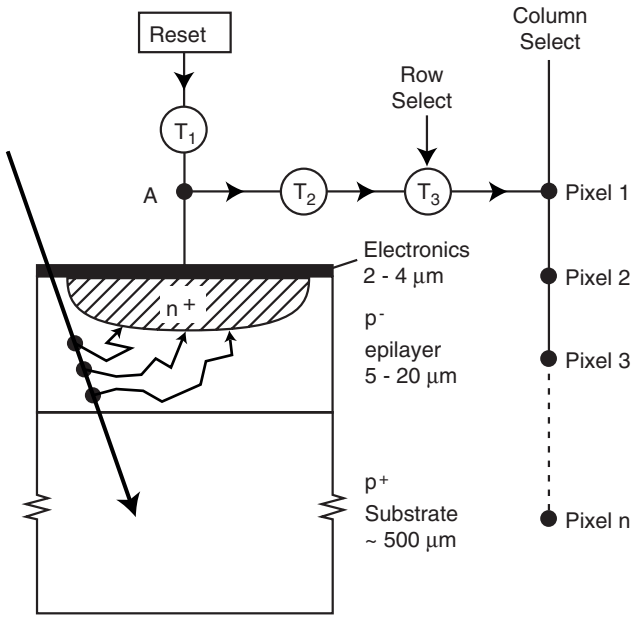

Figure 9. Single pixel schematic for a MAPS pixel. Note that the passivation layer on top of the electronics can make the thickness about 5 μm, which can only be traversed by an electron with greater than 30 keV energy. Reproduced with permission from Faruqi. Copyright 2007 Elsevier.

The general scheme for MAPS readout is shown in figure 10 along with that for a CCD for comparison. Since the CCD has one or at most four readout nodes whilst MAPS could be designed with a node (ADC) on each column, the readout speeds in the latter can be considerably faster. Further comparisons between CCDs and MAPS have been reviewed by (Janesick and Putnam 2003).

4.1. Radiation damage in MAPS

In general CMOS-based sensors suffer from radiation damage as they are exposed to significant doses of radiation even over short periods. Two main types of damage, displacement damage and damage due to charging effects in the diodes (Bogaerts *et al* 2003) are well understood. The former type of damage only occurs at higher energies (>260 keV) and does not concern us in the present application dealing with low energy electrons. The second type of damage is caused by holes being trapped in the oxide layer of the diode causing an increase in the leakage current (dark current). With higher doses of radiation, the dark current in MAPS detectors increases to such an extent that insufficient dynamic range is left to acquire any useful signal (Faruqi *et al* 2005a). Further, the images become noisier as it is more difficult to correct for the additional dark current noise.

For non-rad-hard sensors, radiation damage limits the useful lifetime to 10–20 krad—which is not adequate for putting the sensors into regular usage. However, when the diodes and transistors are designed with enclosed gate geometry (Bogaerts *et al* 2003) the lifetime of the sensor can be extended by many orders of magnitude (Faruqi *et al* 2006).

Evaluation of a radiation hard sensor, the STAR250, designed by FillFactory (http://www.cypress.com) to radiation damage at 300 keV was carried out with electron dose up to ~1 Mrad. The radiation damage to the chip was estimated by measuring the reduction in contrast in the image of an electron microscope grid due to irradiation with a uniform beam of electrons. Imaging the grid for this measurement ensures that part of the sensor gets irradiated whilst an adjacent area is almost unexposed, providing an excellent baseline for separating out the radiation effects. The increase in dark current with irradiation is evident, in both dark and bright field images, in figure 11. However, the damage is much less in evidence if the difference between the bright and dark images is obtained in figure 10(b). The residual contrast at 200 krad is ~87% and at 1 Mrad 82%. It can be concluded that, if care is taken in the dark field corrections, it should be possible to use the MAPS detectors at least up to 1 Mrad. The dosage can be further increased by even limited cooling of the sensor.

5. Summary and conclusions

Both hybrid detectors and MAPS have certain attractive features for low energy electron detection. A hybrid detector such as Medipix2 could be used immediately for low energy electrons. The DQE is expected to be quite high but a careful study needs to be made to establish this as MTF measurements have been done only at 40–120 keV and DQE measurements at 120 keV. Radiation damage is unlikely to be a problem as

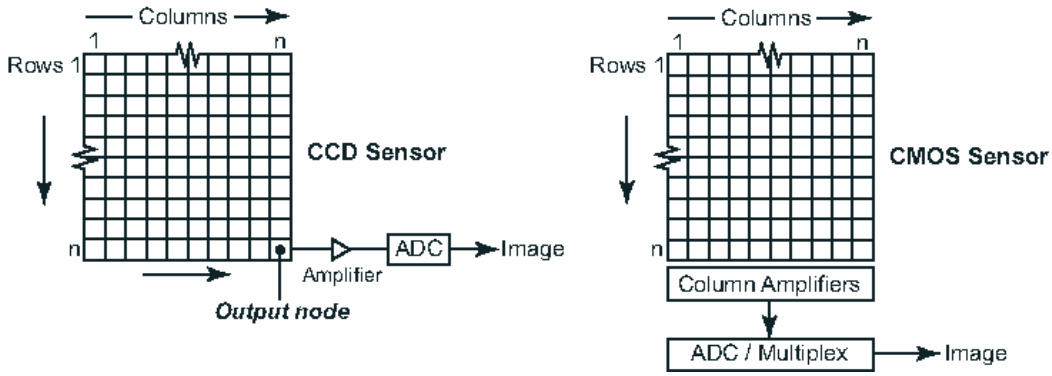

Figure 10. Readout schemes for CCD (left), based on a single node readout. Charge is transferred along the rows before being read out sequentially through the output amplifier into an ADC. On the other hand only voltage pulses are transferred into multiple column amplifiers multiplexed into ADCs—making the readout considerably faster. Reproduced with permission from Faruqi. Copyright 2007 Elsevier.

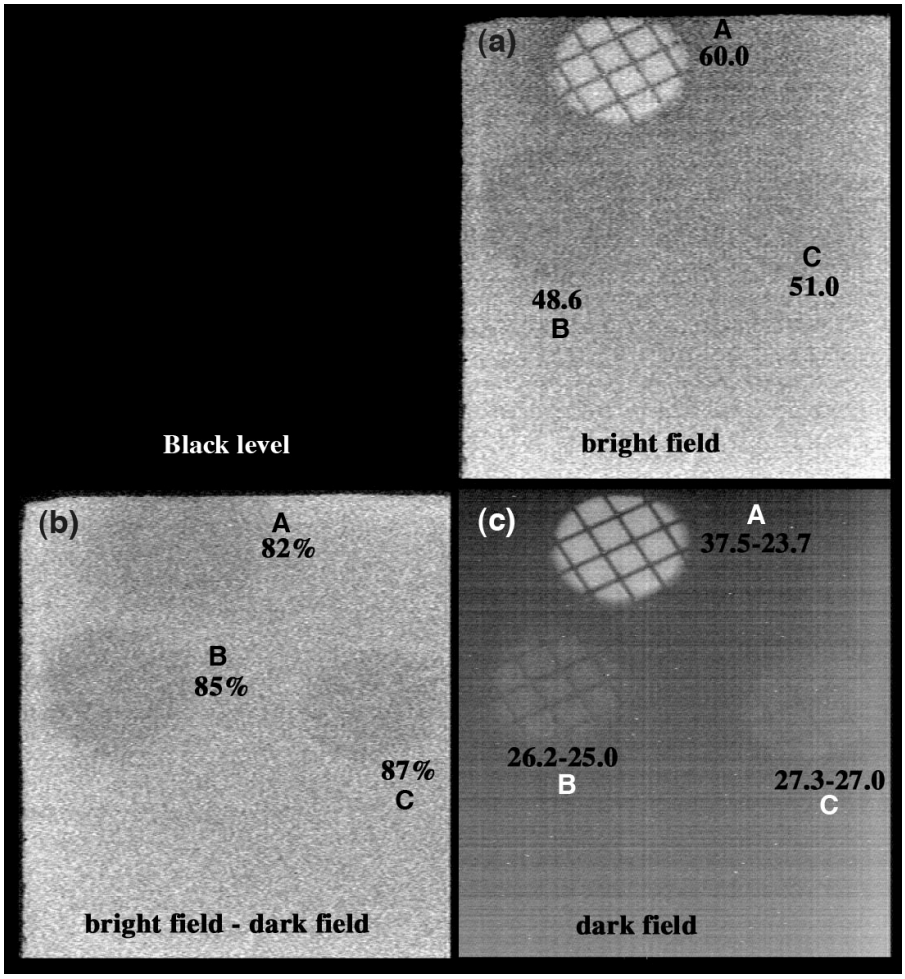

Figure 11. Evaluation of radiation damage in STAR250, which was designed to be rad-hard. Reproduced with permission from Faruqi *et al*. Copyright 2006 Elsevier.

electrons do not penetrate through the sensor to damage the readout chip. The pixel size (55 μm) would be difficult to reduce substantially due to the area occupied by the solder bump and partly due to the amount of pixel readout electronics which is packed rather tightly in the pixel. With improvements in future technology it might become possible to reduce the pixel size in a completely new design.

It is essential to back thin MAPS detectors before they can be used for low energy electron detection. This technology is becoming easily available but requires an extra step in the fabrication of the detector. As the readout for MAPS is analogue, there is some noise added to the signal; this may be reduced by clever design, e.g. using double correlated sampling or different types of reset circuits.

In conclusion, both Medipix2 and MAPS offer attractive features for low energy electron detection. Noiseless readout may be attainable with Medipix2 and much faster readout with MAPS.

References

Bogaerts J, Dierckx B, Meynants G and Uwaerts D 2003 *IEEE Trans. Electron. Devices* **50** 84–90

Cabello J, Bailey A, Kitchen I, Prydderch M, Clark A, Turchetta R and Wells K 2007 *Phys. Med. Biol.* **52** 4993–5011

Cabello J and Wells K 2007 *NSS: Nuclear Science Symp. Conf. Record* vol 5 (Piscataway, NJ: IEEE) pp 3625–30

Deptuch G 2005 *Nucl. Instrum. Methods* **543** 537–48

Deptuch G, Besson A, Rehak P, Szelezniak M, Wall J, Winter M and Zhu Y 2007 *Ultramicroscopy* **107** 674–84

Faruqi A R 2007 *Adv. Imaging Electron Phys.* **145** 55–94

Faruqi A R, Cattermole D M, Henderson R, Mikulec B and Raeburn C 2003 *Ultramicroscopy* **94** 263–76

Faruqi A R and Henderson R 2007 *Curr. Opin. Struct. Biol.* **17** 549–55

Faruqi A R, Henderson R and Holmes J 2006 *Nucl. Instrum. Methods* **565** 139–43

Faruqi A R, Henderson R, Prydderch M, Turchetta R, Allport P and Evans A 2005a *Nucl. Instrum. Methods* **546** 170–5

Faruqi A R, Henderson R and Tlustos L 2005b *Nucl. Instrum. Methods* **546** 160–3

Faruqi A R and Subramaniam S 2000 *Q. Rev. Biophys.* **33** 1–28

Janesick J and Putnam G 2003 *Annu. Rev. Nucl. Part. Sci.* **53** 263–300

Joy D C 1995 *Monte Carlo Modeling for Electron Microscopy and Microanalysis* (Oxford: Oxford University Press)

Llopart X and Campbell M 2003 *Nucl. Instrum. Methods* A **509** 157–63

Llopart X, Campbell M, Dinapoli R, San Secundo D and Pernigotti E 2002 *IEEE Trans. Nucl. Sci.* **49** 2279–83
McMullan G, Cattermole D, Chen S, Henderson R, Llopart X, Summerfield C, Tlustos L and Faruqi A R 2007 *Ultramicroscopy* **107** 401–13
McMullan G, Chen S, Henderson R and Faruqi A R 2008 *Ultramicroscopy* at press
McMullan G and Faruqi A R 2008 *Nucl. Instrum. Methods* A **591** 129–33
Mettivier G, Montesi M C and Russo P 2004 *Nucl. Instrum. Methods* A **516** 554–63
Prydderch M L, Waltham N J, Turchetta R, French M J, Holt R, Marshall A, Burt D, Bell R, Pool P, Eyles C and Mapson-Menard H 2003 *Nucl. Instrum. Methods* A **512** 358–67
Tlustos L, Ballabriga R, Campbell M, Heijne E, Kincade K, Llopart X and Stejskal P 2006 *IEEE Trans. Nucl. Sci.* **53** 367–72